

Enhanced optical absorption in nanopatterned silicon thin films with a nano-cone-hole structure for photovoltaic applications

Qing Guo Du,¹ Chan Hin Kam,^{1,2} Hilmi Volkan Demir,¹ Hong Yu Yu,¹ and Xiao Wei Sun^{1,*}

¹*School of Electrical and Electronic Engineering, Nanyang Technological University, Nanyang Avenue, Singapore 639798, Singapore*

²*e-mail: echkam@ntu.edu.sg*

**Corresponding author: exwsun@ntu.edu.sg*

Received March 14, 2011; accepted April 6, 2011;
posted April 11, 2011 (Doc. ID 144085); published April 29, 2011

In this paper, the optical properties of the silicon nano-cone-hole (NCH) structure array are studied. The ultimate efficiency of the optimized NCH array is enhanced by 23.11% compared to an optimized nanohole array of the same thickness. The absorptance enhancement of the NCH arrays is attributed to its lowered reflectance, more supported resonant modes, and enhanced mode interaction. The angular dependence of ultimate efficiency is also investigated. © 2011 Optical Society of America

OCIS codes: 310.6628, 310.6845, 040.5350.

The silicon solar cell is presently dominating the solar cell market, owing to its abundant supply, nearly ideal band gap, and mature fabrication process. Most commercial silicon solar cells are made from bulk silicon with the thickness of a few hundred micrometers, i.e., a large amount of silicon is consumed, leading to a higher cost for the final product [1]. The thin film silicon solar cell with thicknesses in the range of a few micrometers is a promising way to reduce costs. However, weak absorption, especially in the long wavelength side near the bandgap edge of the silicon, remains a challenge. To address this problem, light trapping techniques, including randomly textured structures [2,3], periodic gratings [4], photonic crystals [5–7], and plasmonic structures [1,8,9], have recently been developed.

Instead of texturing the front and back surface of the solar cells, it is possible to texture the active layer into nanostructured arrays such as with nanowire (NW) [10–14] nanocone (NC) [13], and nanohole (NH) [15] arrays. Theoretical studies [16–20] show that there is a large enhancement of the optical absorption due to efficient antireflection of the incident light and effective optical coupling between nanoarrays and the incident light. It is further demonstrated that NH arrays [19] exhibit stronger optical absorption compared to NW arrays [17,18] with the same filling ratio and thickness. In this Letter, to further increase the optical absorption, we proposed and numerically demonstrated a new nanostructured architecture of nano-cone-hole (NCH) array that enables significantly enhanced absorption, surpassing those of the previously reported arrays.

Figure 1(a) shows the schematic of the proposed NCH array. It can be seen that the NCH array is arranged in a square lattice in the x - y plane and surrounded by air. Sunlight is directly incident on top of the structure along the z direction. The two-dimensional (2D) side and top views are shown in Figs. 1(b) and 1(c), respectively. Considering the fabrication tolerance, the tip of the NCH is not exactly at the bottom surface; instead, a small hole with radius of 20 nm is left on the bottom surface [Fig. 1(b)]. The lattice constant (period) of the square lat-

tice is indicated as a . The radius of the air hole at the top surface is r , and the thickness is h . The air filling ratio (f_{MAX}) is defined as the ratio of the top-surface air hole area to the unit cell surface area, given by $f_{\text{MAX}} = \pi r^2/a^2$. Here the NH array has the same lattice constant a as NCH array and the air filling ratio f of the NH array is defined as in [19]. In our analysis, the thickness h of the NCH and NH arrays is fixed at $2.33 \mu\text{m}$, the same as in [17,19], for easy comparison. The silicon dielectric function used is taken from [21]. The finite-difference time-domain (FDTD) method was employed for all simulations using Lumerical FDTD Solutions, a commercial FDTD software package. Periodic boundary conditions were adopted in the x and y directions, and a perfectly matched layer boundary condition was used in the z direction. The reflectance (R) and transmittance (T) were calculated first, and the absorptance (A) was determined by $A = 1 - R - T$.

In Fig. 2, the absorptance and reflectance of the optimized NCH and NH arrays are presented. The absorptance nonpatterned thin film with an optimized anti-reflective (AR) coating is also presented for reference. From Fig. 2(a), the absorptance of the NCH array is significantly enhanced across the whole wavelength range investigated, except for a narrow range around $0.8 \mu\text{m}$. This implies that the NCH array exhibits a better light trapping property compared to the NH array. In addition to the enhancement of absorptance in the short

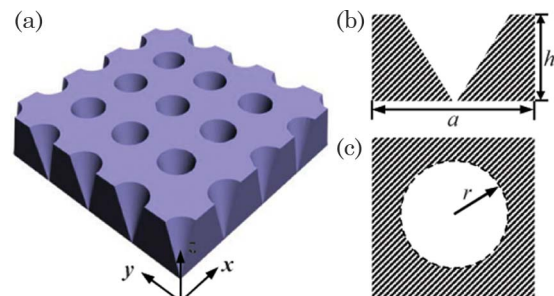


Fig. 1. (Color online) (a) Schematic of the NCH array. (b) 2D side view and (c) top view of the NCH array.

wavelength range, it is worth noting that the absorptance curve of the NCH array shows a large redshift towards the long wavelength, which means that the inefficient absorption in the long wavelength range ($>0.8\ \mu\text{m}$) suffered by thin film solar cells has been alleviated greatly. In the long wavelength range, each peak in the absorptance spectra corresponds to a quasiguided resonant mode [7], and these modes supported by nanostructures help to enhance absorption [7,18,19]. From Fig. 2(a), both the NCH and NH arrays support resonant modes that result in stronger absorptance compared to nonpatterned thin film layers. The NCH array supports more modes compared to the NH array. For the sake of easy visualization, the inset in Fig. 2(a) shows the magnified absorptance spectra of the NCH and NH arrays in the wavelength range from 0.90 to $0.95\ \mu\text{m}$ (indicated by the purple dashed curve). It is clear that more modes (peaks) are supported by the NCH array compared to the NH array, contributing to the further enhancement of the absorptance in the case of the NCH arrays. Besides, the overall absorptance of NCH arrays is also improved compared to the NH arrays, which resulted mainly from a stronger coupling between the incoming light and the supported modes in the NCH structure. The reflectance spectra of the NCH and NH arrays are compared in Fig. 2(b). Thanks to the better gradual changing of the effective refractive index of the NCH arrays [22], it is clear that the reflectance of the NCH array is much lower than that of the NH array in the whole wavelength range, especially for short wavelengths.

Assuming that each photon absorbed by the active layer can generate an electron-hole pair, the ultimate efficiency, η , can be written as [23]

$$\eta = \frac{\int_0^{\lambda_g} I(\lambda)A(\lambda) \frac{\lambda}{\lambda_g} d\lambda}{\int_0^{\infty} I(\lambda)d\lambda}, \quad (1)$$

where $I(\lambda)$ is the solar intensity of the Air Mass 1.5 (AM1.5) direct normal and circumsolar spectrum [24], $A(\lambda)$ is the absorptance, λ is the wavelength, and λ_g is the wavelength corresponding to the bandgap. The efficiency of the NCH array (NH array) is calculated for various a and $f_{\text{MAX}}(f)$, while keeping $h = 2.33\ \mu\text{m}$ for easy comparison.

The ultimate efficiency of the NCH array is shown in Fig. 3(a). For comparison, instead of using the data of [19] directly, we optimized the efficiency of the NH arrays using the FDTD method [Fig. 3(b)]. Our results are very close to those reported in [19]. In Fig. 3(a), we observe that a larger f_{MAX} promises a higher efficiency, regardless

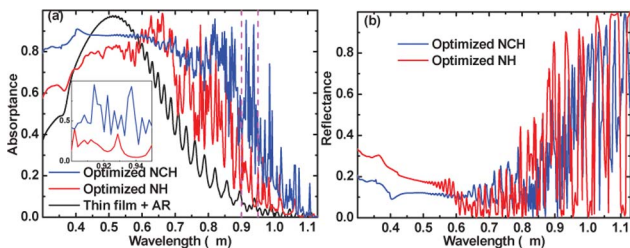


Fig. 2. (Color online) (a) Absorptance of the optimized NCH array and NH array. Inset, enlarged spectra from 0.9 to $0.95\ \mu\text{m}$. (b) Reflectance of the same NCH array and NH array.

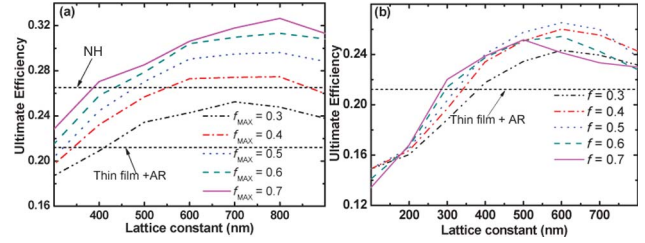


Fig. 3. (Color online) (a) Ultimate efficiency of the NCH array for different lattice constants, a , and maximum filling ratios, f_{MAX} . (b) Ultimate efficiency of the NH array for different lattice constants, a , and filling ratios, f .

of the lattice constant for all NCH arrays. With the increased f_{MAX} , the change of the effective refractive index across the thickness of the NCH arrays in the z direction is more gradual, which results in a better antireflection characteristic, further enhancing the absorption. This can be verified by the absorptance and reflectance spectra for different f_{MAX} with $a = 800\ \text{nm}$ in Figs. 4(a) and 4(b). With the larger f_{MAX} , the absorptance is higher and the reflectance is lower. The influence is more pronounced in the short wavelength range. For all f_{MAX} , the transmittance (which is not shown here) is close to zero in the short wavelength range, which additionally verifies that the antireflection characteristic is more effective in this range. The efficiency increases with the increasing of the lattice constant up to $a = 800\ \text{nm}$, after which the efficiency begins to drop with the further increase of a . More modes are supported for a larger a [18,19], and simultaneously, the reflectance in the short wavelength range increases [20]. The absorptance and reflectance spectra of different a with $f_{\text{MAX}} = 0.7$ are depicted in Figs. 4(c) and 4(d), respectively. With the increased a , the absorptance decreases in the short wavelength range and then increases in the long wavelength range. The resonant modes are mainly contributing to the absorption in the long wavelength range, and the antireflection property dominates in the short wavelength range. There is a trade-off between these two, especially for a larger lattice constant. When a is smaller than $800\ \text{nm}$, more supported

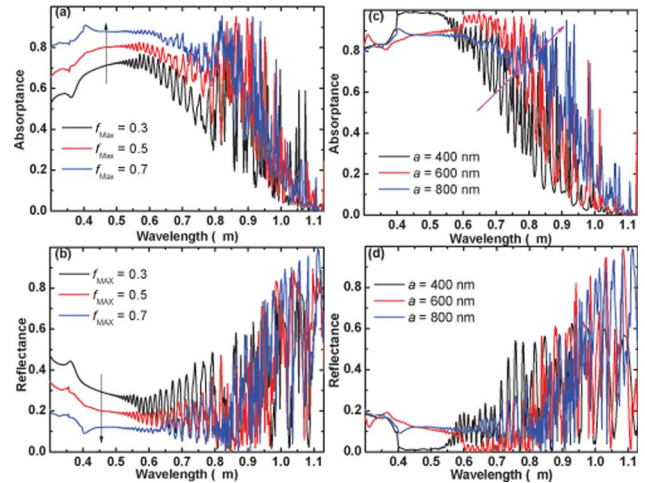


Fig. 4. (Color online) (a) Absorptance and (b) reflectance of the NCH array of different f_{MAX} with $a = 800\ \text{nm}$ and $h = 2.33\ \mu\text{m}$. (c) Absorptance and (d) reflectance of the NCH array of different a with $f_{\text{MAX}} = 0.7$ and $h = 2.33\ \mu\text{m}$.

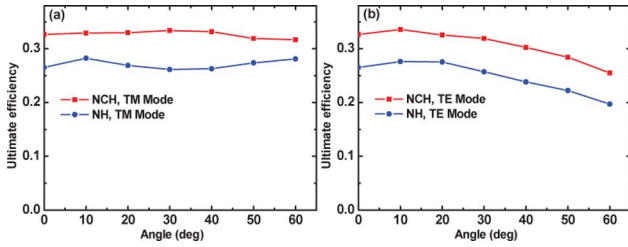


Fig. 5. (Color online) Angular dependence of the ultimate efficiency of the (a) TE and (b) TM modes of the optimized NCH and NH arrays, respectively.

modes help to bring up the efficiency. When a is larger than 800 nm, the mode enhancement will be suppressed by the energy loss in the short wavelength range resulting from an increased reflection. The optimized ultimate efficiency is achieved at 32.65% when $a = 800$ nm and $f_{\text{MAX}} = 0.7$ [Fig. 3(a)]. It is worth noticing that for wavelengths ranging from 600 to 800 nm, the absorptance and reflectance exhibit a nonmonotonic dependence on the lattice constant. For $a = 600$ nm, a better AR performance can be obtained in this wavelength range, but not the ultimate efficiency, which is larger for $a = 800$ nm. This is mainly caused by the contribution in the long wavelength range. The optimized ultimate efficiency of the NH arrays is shown in Fig. 3(b). The relationship between the ultimate efficiency and the design parameters a and f for the NH has been clearly explained [19]. The highest efficiency is 26.52% with $a = 600$ nm and $f = 0.5$ for the NH array (indicated by the black arrows) in Fig. 3(a). Compared to NH arrays, the ultimate efficiency of the NCH arrays is enhanced by 23.11%, surpassing the feasible enhancement using the NH structure.

For the thin film structure, the efficiency can be significantly improved by an AR coating. For example, with an optimized 70 nm Si_3N_4 , the ultimate efficiency of the AR thin film solar cell is increased to 21.21%, which has been enhanced by 36.84% compared to that of the thin film without the AR coating (15.50%). Here, we also investigate the influence of the AR coating for the optimized NCH and NH arrays. The dielectric function of Si_3N_4 is taken from [5]. The efficiency of the NCH and NH arrays is increased to 34.23% and 28.83%, respectively, with optimized AR coating thicknesses of 73 and 63 nm, respectively. The efficiency of the NCH array is enhanced by 18.73% compared to the NH array, which is still significant. The AR coating mainly contributes to the improvement of absorptance in the short wavelength range. The modes supported by the NCH and NH arrays are not influenced by the AR coating.

In Figs. 5(a) and 5(b), we show the angular dependence of the ultimate efficiency for the optimized NCH and NH arrays, respectively. For both the NCH and NH arrays, TM polarization has higher ultimate efficiency than TE polarization. For the incident angles up to 60°

that we simulated, the NCH array always showed better efficiency than the NH array.

In conclusion, we presented a new NCH array structure with the highest ultimate efficiency of 32.65%, which is much larger than that can be obtained by the NH array. The optical properties of the NCH array are analyzed in detail. Lower surface reflectance, more supported resonant modes, and enhanced modes interaction are the main reasons for the significantly enhanced absorption of the NCH array. The NCH array has better ultimate efficiency than the NH array, even for large incident angles up to 60°.

References

1. K. R. Catchpole and A. Polman, *Opt. Express* **16**, 21793 (2008).
2. E. Yablonovitch and G. D. Cody, *IEEE Trans. Electron Devices* **29**, 300 (1982).
3. Z. Yu, A. Raman, and S. Fan, *Proc. Natl. Acad. Sci. USA* **107**, 17491 (2010).
4. Z. Yu, A. Raman, and S. Fan, *Opt. Express* **18**, A366 (2010).
5. L. Zeng, Y. Yi, C. Hong, J. Liu, N. Feng, X. Duan, L. C. Kimerling, and B. A. Alamariu, *Appl. Phys. Lett.* **89**, 111111 (2006).
6. P. Bermel, C. Luo, L. Zeng, L. C. Kimerling, and J. D. Joannopoulos, *Opt. Express* **15**, 16986 (2007).
7. S. B. Mallick, M. Agrawal, and P. Peumans, *Opt. Express* **18**, 5691 (2010).
8. V. E. Ferry, L. A. Sweatlock, D. Pacifici, and H. A. Atwater, *Nano Lett.* **8**, 4391 (2008).
9. H. A. Atwater and A. Polman, *Nat. Mater.* **9**, 205 (2010).
10. N. S. Lewis, *Science* **315**, 798 (2007).
11. B. Tian, X. Zheng, T. J. Kempa, Y. Fang, N. Yu, G. Yu, J. Huang, and C. M. Lieber, *Nature* **449**, 885 (2007).
12. M. D. Kelzenberg, D. B. Turner-Evans, B. M. Kayes, M. A. Filler, M. C. Putnam, N. S. Lewis, and H. A. Atwater, *Nano Lett.* **8**, 710 (2008).
13. J. Zhu, Z. F. Yu, G. F. Burkhard, C. M. Hsu, S. T. Connor, Y. Q. Xu, Q. Wang, M. McGehee, S. H. Fan, and Y. Cui, *Nano Lett.* **9**, 279 (2009).
14. M. D. Kelzenberg, S. W. Boettcher, J. A. Petykiewicz, D. B. Turner-Evans, M. C. Putnam, E. L. Warren, J. M. Spurgeon, R. M. Briggs, N. S. Lewis, and H. A. Atwater, *Nat. Mater.* **9**, 368 (2010).
15. K.-Q. Peng, X. Wang, L. Li, X.-L. Wu, and S.-T. Lee, *J. Am. Chem. Soc.* **132**, 6872 (2010).
16. B. M. Kayes, H. A. Atwater, and N. S. Lewis, *J. Appl. Phys.* **97**, 114302 (2005).
17. L. Hu and G. Chen, *Nano Lett.* **7**, 3249 (2007).
18. C. X. Lin and M. L. Povinelli, *Opt. Express* **17**, 19371 (2009).
19. S. E. Han and G. Chen, *Nano Lett.* **10**, 1012 (2010).
20. F. Wang, H. Yu, J. Li, X. Sun, X. Wang, and H. Zheng, *Opt. Lett.* **35**, 40 (2010).
21. E. D. Palik, *Handbook of Optical Constants of Solids*, Vol. 1 (Academic, 1998).
22. M. J. Minot, *J. Opt. Soc. Am.* **66**, 515 (1976).
23. W. Shockley and H. J. Queisser, *J. Appl. Phys.* **32**, 510 (1961).
24. American Society for Testing and Materials, "Air Mass 1.5 Spectra," retrieved from <http://rredc.nrel.gov/solar/spectra/am1.5/>.